Propagation of pacemaker activity in the guinea-pig antrum

G. W. Hennig, G. D. S. Hirst, K. J. Park, C. B. Smith, K. M. Sanders, S. M. Ward and T. K. Smith

Department of Physiology and Cell Biology, University of Nevada School of Medicine, Reno, Nevada, 89557, USA

Cyclical periods of depolarization (slow waves) underlie peristaltic contractions involved in mixing and emptying of contents in the gastric antrum. Slow waves originate from a myenteric network of interstitial cells of Cajal (ICC-MY). In this study we have visualized the sequence and propagation of Ca^{2+} transients associated with pacemaker potentials in the ICC network and longitudinal (LM) and circular muscle (CM) layers of the isolated guinea-pig gastric antrum. Gastric antrum was dissected to reveal the ICC-MY network, loaded with Fluo-4 AM and activity was monitored at 37°C. Ca^{2+} waves propagated throughout the ICC-MY network at an average velocity of 3.24 ± 0.12 mm s^{-1} at a frequency of 4.87 ± 0.16 cycles min^{-1} ($n = 4$). The propagation of the Ca^{2+} wave often appeared 'step-like', with separate regions of the network being activated after variable delays. The direction of propagation was highly variable (Δ angle of propagation 44.3 ± 10.9 deg per cycle) and was not confined to the axes of the longitudinal or circular muscle. Ca^{2+} waves appeared to spread out radially from the site of initiation. The initiating Ca^{2+} wave in ICC-MY was correlated to secondary Ca^{2+} waves in intramuscular interstial cells of Cajal, ICC-IM, and smooth muscle cells, and the local distortion (contraction) in a field of view. TTX (1 μM) had little effect on slow wave or pacemaker potential activity, but 2-APB (50 μM) blocked all Ca^{2+} waves, indicating a pivotal role for intracellular Ca^{2+} stores. Nicardipine (2 μM) eliminated the Ca^{2+} transient generated by smooth muscle, but did not affect the fast upstroke associated with ICC-MY. These results indicate that slow waves follow a sequence of activation, beginning with the ICC-MY and ICC-IM network, followed later by a sustained Ca^{2+} transient in the muscle layers that is responsible for contraction.

(Received 8 December 2003; accepted after revision 29 January 2004; first published online 30 January 2004)
Corresponding author T. K. Smith: Department of Physiology and Cell Biology, University of Nevada School of Medicine, Reno, Nevada, 89557, USA. Email: tks@physio.unr.edu

Underlying many gastrointestinal motor patterns are cyclical electrical slow waves that determine the frequency and force of phasic contractions in the gastrointestinal (GI) tract. Originally thought to be a property of the smooth muscle cells (Tomita, 1981; Sanders & Publicover, 1989), more recent work has shown that the cells responsible for the generation of slow waves are interstitial cells of Cajal (ICC; Langton *et al.* 1989; Ward *et al.* 1994; Huizinga *et al.* 1995; Torihashi *et al.* 1995; Sanders, 1996; Dickens *et al.* 1999; Ordog *et al.* 1999). In the gastric antrum, ICC located in the plane of the myenteric plexus, between the longitudinal and circular muscle layers (ICC-MY) generate pacemaker potentials, which are conducted, with decrement, to the adjacent layers of smooth muscle (Dickens *et al.* 1999; Cousins *et al.* 2003). The generation of complete slow waves in the circular layer involves intramuscular ICC (ICC-IM; Dickens *et al.* 2001) and may also involve ICC that lie in septa between muscle bundles (ICC-SEP: Horiguchi *et al.* 2001). Depolarization of ICC and smooth muscle during the slow wave cycle initiates Ca^{2+} entry via L-type Ca^{2+} channels in ICC and smooth muscle cells and additionally by dihydropyridine-resistant Ca^{2+} channels in ICC-MY (Lee & Sanders, 1993; Hirst & Edwards, 2001; Kim *et al.* 2002; Kito *et al.* 2002). Thus, techniques to measure oscillations in intracellular Ca^{2+} at the frequency of electrical slow waves are means of monitoring these events.

ICC-MY are electrically coupled via gap junctions and form a continuous electrical network in the stomach from the proximal corpus to the pylorus. However, there are heterogeneities in the density of the ICC network in different regions of the stomach (Hirst *et al.* 2002*a*; Ordog *et al.* 2002). The spread of slow waves, and thus the organization of gastric contractions, is dependent upon the continuity and function of the ICC-MY network and the intrinsic pacemaker frequency gradient in which

 DOI: 10.1113/jphysiol.2003.059055

corpus ICC-MY generate pacemaker potentials at a higher frequency than do more distal pacemakers (Ordog *et al.* 2002). Gastric muscles lacking ICC-MY do not generate electrical slow waves, and muscles with partial loss of ICC-MY do not actively propagate slow waves through regions devoid of ICC-MY (Ordog *et al.* 1999). Little is known about the propagation of slow waves through ICC-MY networks; however, recent studies have suggested that voltage-dependent Ca^{2+} entry may entrain pacemakers from one cell to the next (Hirst & Edwards, 2001; Kim *et al.* 2002). It is also possible that voltage-dependent activation of phospholipase C could participate in entrainment of pacemakers (Nose *et al.* 2000). Measuring latencies between slow waves at multiple points in small sheets of gastric muscle and applying triangulation algorhythms has shown that pacemaker initiation is not anatomically fixed to a single site; the site of origin of slow waves can shift from cycle-to-cycle (Publicover & Sanders, 1984). Direct visualization of ICC-MY activity, with Ca^{2+} imaging of the mouse ileum (Yamazawa & Iino, 2002), has demonstrated the feasibility of using optical techniques to investigate the frequency, propagation velocity, and sequence of activation of ICC *in situ*. Ca^{2+} imaging has been particularly helpful in understanding the spread of excitability through smooth muscle layers (see Stevens *et al.* 1999, 2000; Hennig *et al.* 2002). A combination of these techniques may be useful in studying the interactions and sequence of activation between ICC-MY and smooth muscle cells.

Here we have used video-rate Ca^{2+} imaging techniques to investigate the characteristics of slow wave propagation in networks of gastric ICC-MY and the spread of activity from ICC-MY to smooth muscle cells in the guinea-pig gastric antrum. We have measured cell-to-cell spread of Ca^{2+} waves that occur at the frequency of gastric slow waves. These measurements have been analysed to study the sequence of activation of ICC-MY within a localized network and the spread of activity to circular muscle cells and ICC-IM.

Methods

Tissue preparation

Guinea-pigs of either sex, weighing between 150 and 250 g were killed by isoflurane inhalation followed by exsanguination, in accordance with the requirements of the Animal Ethics Committee at the University of Nevada, Reno, USA.

A ventral midline incision was made to expose the peritoneal cavity, and a strip of gastric antrum was removed along the greater curvature. After flushing with oxygenated (97% O_2–3% CO_2) Krebs solution (composition (mM): NaCl 120.35, KCl 5.9, $NaHCO_3$ 15.5, $MgCl_2$ 1.2, NaH_2PO_4 1.2, $CaCl_2$ 2.5, D-glucose 11.5, pH 7.4), the mucosa and submucosa were peeled away and the tissue was pinned serosal side topmost. The serosa and longitudinal muscle were carefully peeled away from the circular muscle (Hirst & Edwards, 2001). Sometimes the myenteric plexus and ICC-MY network remained attached to the longitudinal muscle, in which case, these preparations were pinned serosal side down in an organ bath containing Krebs solution at $36.5 \pm 0.5^{\circ}$C. If the myenteric plexus and ICC-MY network remained attached to the circular muscle side, these preparations were pinned luminal side down, so as to always orientate the ICC-MY network topmost. The tissue was equilibrated for 1–1.5 h, during which time, rhythmical contractions became prevalent.

Fluorescent dye loading

After equilibration, the preparation was incubated with 5 μM Fluo-4 AM (FluoroPure(TM) or cell permeant, special packaging: Molecular Probes, Eugene, OR, USA), 0.02% dimethyl sulfoxide and 0.01% non-cytotoxic detergent cremophor EL (Sigma, St Louis, MO, USA), for 16 min at $25 \pm 2^{\circ}$C. Following incubation, the tissue was perfused with Krebs solution ($35 \pm 0.5^{\circ}$C) for 20–30 min to allow for de-esterification and re-establishment of phasic contractions.

Drugs

Nicardipine, nifedipine, and tetrodotoxin (TTX) were purchased from Sigma (St Louis, MO, USA). 2-Aminoethyl diphenylborate (2-APB) was purchased from Tocris (Balwin, MO, USA).

Visualization of Ca^{2+} transients in ICC

The preparation was viewed under an Olympus BX50WI (Olympus, Melville, NY, USA) microscope fitted with epi-fluorescence. A number of lenses were used depending on the size of the tissue in which Ca^{2+}-induced fluorescence was being visualized (air lenses: × 2 PlanApo; × 4 UplanFl; water immersion lenses; × 10, × 20, × 40, × 60: Olympus UMPlanF). A wide interference blue filter cube (U-MWIB) produced excitation between 460 and 490 nm, and emission above 515 nm, suitable for Fluo-4 AM (peaks: excitation 490 nm, emission 515 nm). For visualization of Kit immunoreactive cells, a Texas Red filter set was used (41004: Chroma). Ca^{2+}-induced

fluorescence was recorded using an iCCD camera (adapter: Olympus U-TV1 X; camera: IC-300B, Photon Technology International, Monmouth Junction, NH, USA) onto digital video deck (DHR-1000: Sony Corporation, Japan). Camera voltage and gain were adjusted at the beginning of each experiment to provide the maximum range of fluorescence intensity without over-saturation of the signal.

Visualization of ICC cells using c-Kit labelling

After Ca^{2+} fluorescence was recorded from an active region, nifedipine (1 μM) was added to minimize contractile activity and movement. Anti-Kit antibody (ACK-2; Ward *et al.* 1994) was preconjugated to a fluorescent label using a 594 Tagging Kit (Molecular Probes). ACK-2-tagged antibody (3 μl (1 ml)$^{-1}$ Krebs solution; 100 μl) was applied to the stabilized preparations every 10 min (3 times; 30 min total). The preparation was then washed continuously for 15 min with Krebs solution containing nifedipine (1 μM). Labelled ICC were visualized (peaks: excitation 560 nm, emission 645 nm; Filter Set 41004, Chroma Technology Corp, Rockingham, VT, USA) and compared with the positions of cells from which Ca^{2+}-dependent fluorescence signals were previously recorded.

Image processing and analysis

Video clips were captured using a DV (IEEE-1394) interface to a Macintosh G4 Computer (Apple Computers, Cupertino, CA, USA). Video frames (720 × 480 pixels) were converted to 8-bit grayscale and were stored as an image sequence using a modified version of NIH Image 1.62 (NIH, Bethesda, MD, USA).

Some image sequences were de-interlaced by extracting odd and even lines from a single image to create two separate images. This effectively doubled temporal resolution from NTSC-DV 29.97 frames s^{-1} to de-interlaced 59.94 frames.s^{-1} (16.7 ms per image), at the expense of halving vertical resolution. Image processing techniques used in this study are summarized in the Appendix.

Analysis of the spread of pacemaker activity

Analysis of the propagation of waves of pacemaker activity was difficult due to the dim Ca^{2+}-induced fluorescence when using low power lenses (× 2–× 10). At these low magnifications, the intensity of Ca^{2+}-induced fluorescence was extremely faint and required a high camera gain to be employed. This increased the quantum (or 'shot') noise of the resulting image and prevented the use of subtraction techniques (differentiation, background subtraction: see Hennig *et al.* 2002). However, like white noise, the overall average of quantum noise remained constant, thereby making it suitable for spatio-temporal analysis where considerable averaging occurs (Hennig *et al.* 2002).

Radial averaging

The spread of activity through the ICC-MY network was not confined to the orthogonal axes of the longitudinal or circular muscle, making it unsuitable for use of a fixed angle of averaging (Hennig *et al.* 2002) in the creation of spatio-temporal maps. Instead, the angle of averaging was changed from 0 to 180 deg (in increments of 1 deg = 180 spatio-temporal maps) to ensure all possible directions of propagation were accounted for. Out of all the angles of averaging, the one that ran most parallel to the wave front was identified, as it had the highest proportion of bright averaged pixels (little quiescent background included in the average). This map showed the progression of pacemaker activity over time and was used to determine the velocity of propagation (mm s^{-1}). The direction of propagation was determined by calculating the angle perpendicular (at right angles) to the previously determined wave front angle.

Motion stabilization and distortion measurements

The passage of Ca^{2+} waves through the tissue produced noticeable movement. During measurement of Ca^{2+} transients in ICC-MY cells, it was imperative that the cell remain fixed in the same position. To accomplish this, tracking routines were used to follow the *XY* position of a cell, or features near the cell (see Hennig *et al.* 2002). The image sequence was then stabilized so that regions of interest remained in the same position.

To measure the change in surface area (distortion) of a region of tissue, three or four points were tracked to form a triangle or quadrangle, respectively. The change in surface area within the triangle/quadrangle was calculated.

Sequence of activation of different regions and cells of the ICC-MY network

At higher magnifications, it was possible to discern the structure of individual cells in ICC-MY networks with Ca^{2+}-induced fluorescence. By differentiating the image sequence (Hennig *et al.* 1999, 2002), only those structures undergoing rapid changes in fluorescence (see Results)

were highlighted, thereby removing resting, background and slow changes in fluorescence from each image in a sequence. The delay between activation of individual cells and regions of ICC-MY networks was calculated directly from the differentiated image sequence.

Time courses of activity

To determine the time course of Ca^{2+} transients in ICC-MY, image sequences were stabilized, and a cell of interest or a region of interest was outlined. The Ca^{2+}-induced fluorescence intensity was averaged within the outline, and plotted as a time course.

Statistics

Statistical comparisons were made using ANOVA with Newman-Keuls *post hoc* tests. A probability of less than 0.05 was considered significant. *n* refers to the number of animals used.

Results

ICC in guinea-pig antrum identified by Kit labelling

Labelling of ICC with Kit antibody revealed two distinct ICC morphologies in the guinea-pig gastric antrum as previously reported (Burns *et al.* 1997). These cells were located at different planes of focus within the tunica

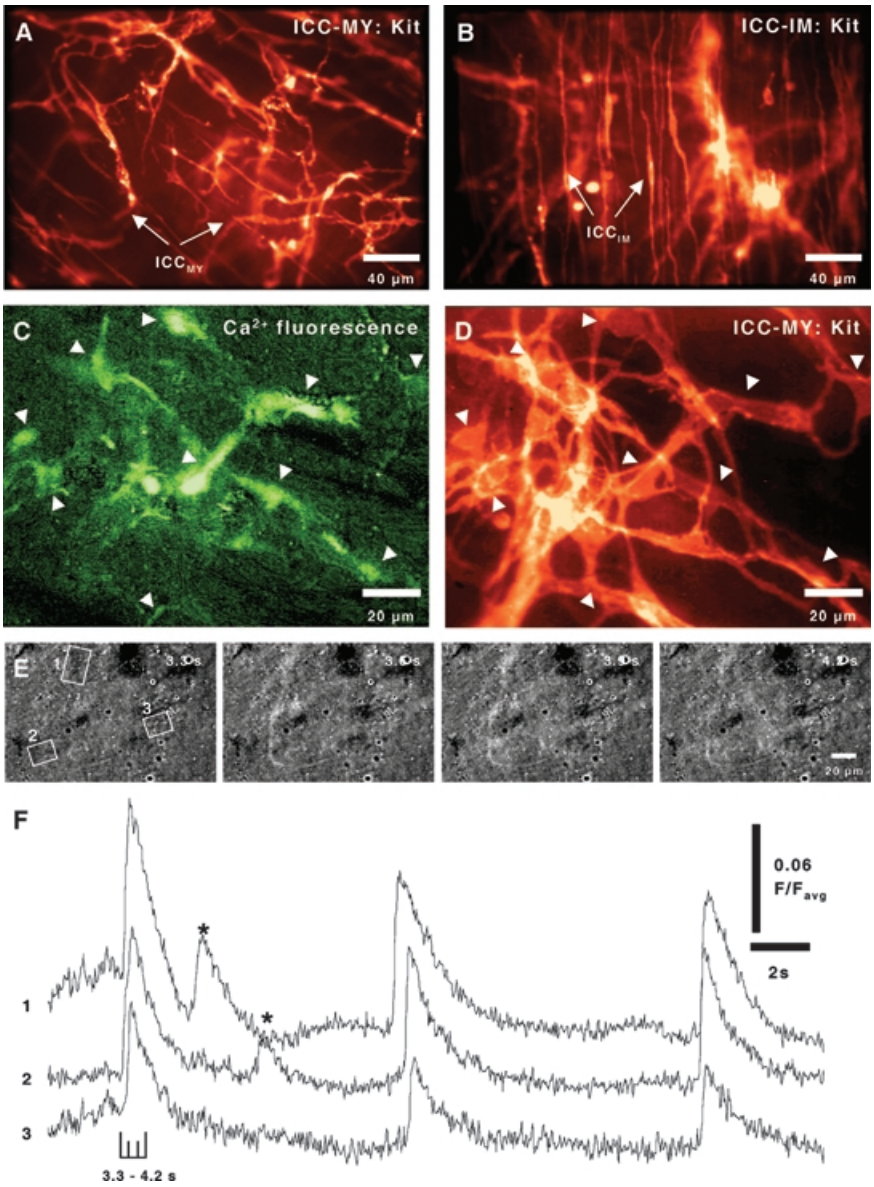

Figure 1. ICC networks loaded with Fluo-4 in the gastric antrum
A, ICC-MY networks were labelled with Kit antibody. ICC-MY (arrows) are multibranching cells that are organized into a network. *B*, ICC-IM (arrows) in the circular muscle layers were also labelled by Kit antibodies. *C*, ICC were loaded with Fluo-4 and underwent fluorescence oscillations at the frequency of slow wave activity. *D*, Kit immunofluorescence confirmed that cells undergoing changes in Ca^{2+} fluorescence (Fluo-4 in *C*) were ICC (compare arrowheads). *E* shows a Ca^{2+} transient cycle at 300 ms intervals in individual ICC loaded with Fluo-4. Active cells are outlined in the panels. *F*, Ca^{2+} oscillations in the ICC outlined in *E*. In some cells spontaneous small transients occurred during the interval between slow waves (∗).

muscularis. One ICC network was composed of irregularly shaped cells arranged in a mesh-like, non-orthogonal fashion. These had the structure of the myenteric network of ICC (ICC-MY; Fig. 1*A*). Within the circular muscle (CM), elongated spindle-shaped cells were arranged in parallel with circular muscle fibres and corresponded to intramuscular ICC (ICC-IM; Burns *et al.* 1996; Fig. 1*B*).

To verify that Ca^{2+} transients could be recorded from ICC-MY, we performed sequential double labelling experiments with Fluo-4 and fluorescently tagged Kit antibodies. In these experiments, a region of tissue was imaged to display Ca^{2+}-dependent fluorescence (Fig. 1*C*), and then the same region was visualized after applying fluorescently tagged Kit antibody (see Methods; Fig. 1*D*). This verified that Ca^{2+} transients recorded from cells with the appearance of ICC-MY were indeed ICC.

Visualization of Ca^{2+} dependent fluorescence in ICC

Imaging Ca^{2+}-induced fluorescence (Fig. 1*F*) in ICC-MY at video rates showed rhythmic Ca^{2+} transients in ICC at an average frequency of $4.87 \pm 0.16\ \text{min}^{-1}$ (interval 12.32 ± 0.4 s at 37°C, $n = 4$; Fig. 1*E*, *F*). This frequency is similar to the frequency of slow waves in the gastric antrum, as previously reported (e.g. Dickens *et al.* 1999). In single cells within the ICC network, Ca^{2+} transients consisted of a rapid upstroke followed by a relatively rapid restoration to baseline (~1.6 s), several secondary Ca^{2+} transients, or a sustained 'plateau-like' enhancement in Ca^{2+} that persisted for several seconds. The periodic Ca^{2+} transients occurred spontaneously without extrinsic stimulation and spread through the network of ICC-MY at an average velocity of $3.24 \pm 0.12\ \text{mms}^{-1}$ ($n = 4$ preparations; 12 fields of view). This propagation velocity is similar to propagation velocities of slow waves in gastric antral muscle strips (Bauer *et al.* 1985), the velocity of propagation of pacemaker potentials in ICC-MY (Hirst *et al.* 2002*a*), and the velocity of antral contractions in the guinea-pig stomach (Hennig *et al.* 1997).

The initial Ca^{2+} wave through ICC-MY often consisted of a single rapid increase in fluorescence (maximum rate $0.664 \pm 0.089\ F/F_{avg}\ s^{-1}$; average rate $0.171 \pm 0.028\ F/F_{avg}\ s^{-1}$), reaching a peak in 284 ± 16 ms (fluorescence at peak $0.075 \pm 0.012\ F/F_{avg}$). The peak was followed by a decay in fluorescence with an average time constant of 0.48 ± 0.07 s ($n = 7$), with restoration of basal Ca^{2+} in 1.58 ± 0.15 s (average rate $-0.026 \pm 0.005\ F/F_{avg}\ s^{-1}$; cells = 6, $n = 5$; Fig. 1*F*). Cells showing this simple profile of activity were in some cases integrated into networks of cells with plateaus or multiple peaks of Ca^{2+} fluorescence following the initial Ca^{2+} upstroke, as described in the previous paragraph.

Propagation velocity of Ca^{2+} wave fronts through ICC-MY networks was not constant as evidenced by regions in which waves propagated faster or slower (Fig. 2*A* and *B*1-4). Often the Ca^{2+} oscillations were more intense in some regions than in others, usually near and around myenteric ganglia. At higher magnifications, distinct layers of the ICC-MY network were observed to be activated non-uniformly (Fig. 2*C*), suggesting that propagation of the Ca^{2+} wave front may travel with some independence through regions of the ICC-MY network above and below myenteric ganglia (Burns *et al.* 1996). The Ca^{2+} waves in Figs 2*A* and *B* are examples of events in which the initial Ca^{2+} wave was followed by a secondary 'plateau-like' Ca^{2+} event, as described above (see inset in Fig. 2).

The direction of Ca^{2+} waves through a field of view was not uniform, and varied from cycle-to-cycle, similar to the changes of direction of spontaneous slow wave activity in strips of gastric muscle (Publicover & Sanders, 1984). Interestingly, the direction of spread of Ca^{2+} waves in ICC-MY was also not confined to the orthogonal axes of either the longitudinal or circular muscle, and Ca^{2+} transients propagated in any direction through the ICC-MY network (Fig. 3). By forming a series of spatio-temporal maps by averaging of pixel intensity within each frame at different angles to the vertical (radial averaging; see Methods) the conduction velocity of the wave and its direction of propagation could be determined. The pixel intensity of the wave front was maximal when averaging occurred parallel to the wave front and was minimal when averaging occurred perpendicular to the wave front (Fig. 3*B*–*D*). The average change in direction per cycle was 44.3 ± 10.9 deg, with the direction remaining stable for 1.6 ± 0.2 cycles ($n = 4$ muscles; 11 fields of view).

The instability in the direction of propagation suggested that the wavefront may spread radially from the site of initiation. Indeed, curvature of the Ca^{2+} wavefronts was often apparent in spatio-temporal maps, where discrete bright areas (angle of averaging in parallel to wavefront) were observed (Fig. 3*B*). Curvature of the spread of Ca^{2+} waves is also shown in Fig. 4.

At low magnification (× 10) it was possible to follow the sequence of activation in the ICC-MY network (Fig. 4). Recordings of multiple Ca^{2+} waves further underscored the variability in the site of origin and the direction of the spread of Ca^{2+} waves. Figure 4 shows an example of 4 cycles in which Ca^{2+} waves spread along specific paths across the field of view, and during 3 cycles, from a site

within the field of view. Collisions of activity spreading from different points of origin anihilated each other (e.g. Fig. 4*B*), demonstrating that cells became refractory after the onset of Ca^{2+} transients. Topological maps were constructed to describe the sequence of activation and the direction of propagation.

The density of the ICC network often made it difficult to unequivocally distinguish individual ICC (see also Burns *et al.* 1997). However, at higher magnification (i.e. × 60), the individual cells could be visualized, allowing analysis of the sequence of activation through small regions of the ICC-MY network (Fig. 5). During the passage of a Ca^{2+} waves, many ICC-MY were activated within a short period of time (e.g. 100 ms), and cells were not activated in a strictly serial fashion. The exact sequence of activation tended to follow different paths through an ICC-MY network from wave to wave, suggesting that entrainment of pacemaker activity cell-to-cell is dynamic. A delay between the initiation of Ca^{2+} waves in cells at different positions in a field of view could be detected even at high magnification, indicating the time dependence (i.e. latency) of the spread of Ca^{2+} waves (Fig. 5*C*; see also sequence in Fig. 1*F*).

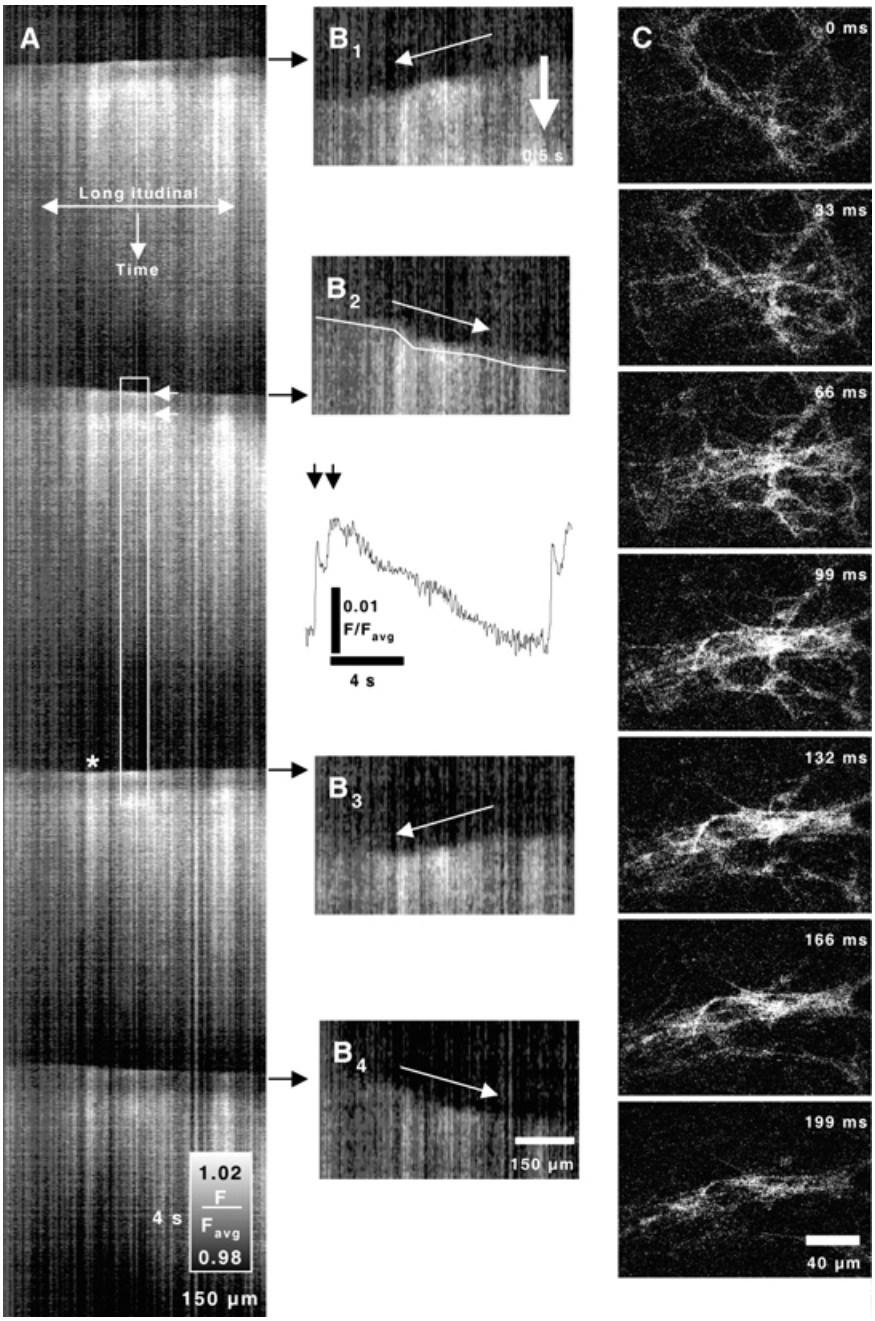

Figure 2. Variability in direction of propagation of slow waves
The direction of propagation of Ca^{2+} waves in the ICC-MY network varied from event to event, with subsequent waves often reversing direction. *A* shows a spatio-temporal map (distance and time as noted) of four Ca^{2+} waves through a network of ICC-MY and the underlying smooth muscle cells. Each wave front consisted of a sharp increase in fluorescence, followed by a partial decrerase and then a sustained increase in fluorecence. This shows up in the spatio-temporal maps as a distinct band along the top of each wave front (see upper white arrow). *B* shows close ups of the leading edges of the Ca^{2+} waves. Arrows denote direction of propagation of each wave. The intensity of the propagating wave was not uniform and varied in different regions (see asterisk in *A*). Similarly, the velocity of propagation showed variation, with periods of retardation or accelaration visualized as 'steps' on the wavefront (white line *B*2). Trace in the inset under B2 shows average relative fluorescence during a single wave at the time noted by the white rectangle in *A*. Two distinct peaks were noted (arrows). At higher magnification, it was possible to distinctly visualize the ICC-MY network, but at this level of resolution, it became more difficult to detect the direction or velocity of propagation (*C*). In some regions, such as around ganglia, different layers of the network activated asynchronously, suggesting multiple propagation pathways can emerge as the pacemaker activity spreads.

Time course and sequence of Ca^{2+} transients in different cell types

Consistent with the hypothesis that ICC-MY are pacemaker cells, spontaneous Ca^{2+} transients in ICC-MY usually initiated Ca^{2+} transients in cells within the muscle layers. Responses in circular and longitudinal muscle cells were detected within 50 ms and consisted of a slow increase in fluorescence (average rate 0.039 ± 0.009 $F/F_{avg}\,s^{-1}$) that reached a peak in 2.90 ± 0.28 s (cells = 7, n = 7; compared to ICC-MY Ca^{2+} transients: time to peak ~10 times slower, average upstroke rate 4.4 times slower, maximum upstroke rate 17 times slower, Fig. 6). Initial fast upstrokes in Ca^{2+} fluorescence (as seen in ICC-MY) were not observed in smooth muscle cells. When Ca^{2+} transients occurred sequentially in ICC-MY and smooth muscle cells, there was a prolongation in the duration of the Ca^{2+} transient in ICC-MY that reflected the time course of the transients in the two cell types (i.e. the initial fast upstroke in Ca^{2+} fluorescence was followed by a slower plateau-like increase; see Figs 6 and 2*B*, inset). Movement of the muscles (Δ surface area) mirrored Ca^{2+} transients in smooth muscle cells, and the slowly developing contraction peaked at approximately the same point in time as the Ca^{2+} transient (Fig. 6*F*).

Cells with the morphology and distribution of ICC-IM (see Fig. 1) were also coupled to the activation of ICC-MY and displayed rapid Ca^{2+} upstrokes in synchrony (average time delay of 48 ± 15 ms, n = 4) with the initial Ca^{2+} transients in ICC-MY (Fig. 6*C*). The initial Ca^{2+} was of

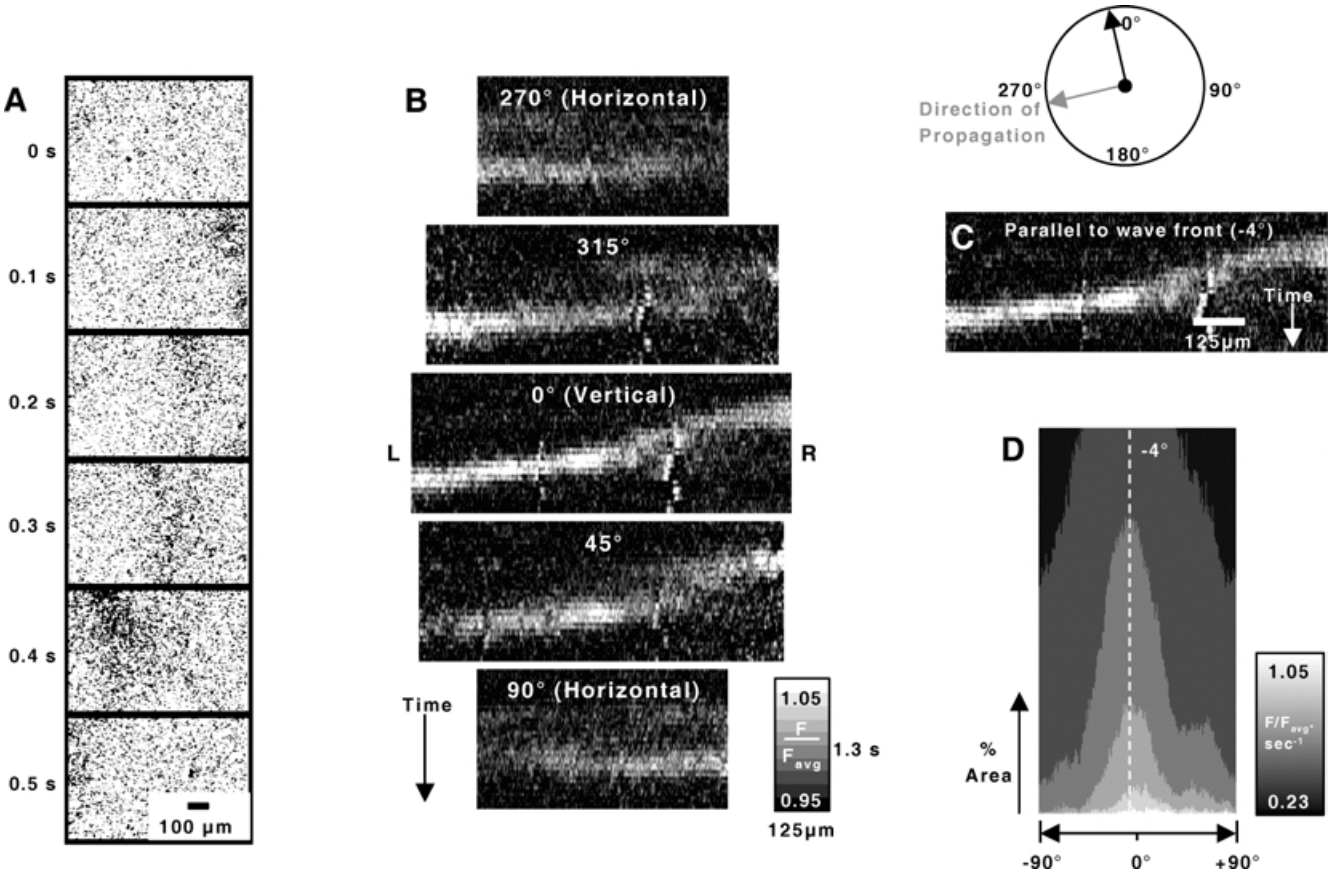

Figure 3. Method to determine direction of propagation
At low magnification the propagation of Ca^{2+} waves in ICC-MY networks was difficult to visualize due to the faint signals (*A* shows a sequence of images depicting the passage of a waves at × 10; image reversed such that black represents an increase in fluorescence). Radial averaging was used to determine the angle at which the Ca^{2+} wave front was parallel to the line of averaging (*B* shows spatio-temporal maps calculated every 45 deg spanning 180 deg), allowing calculation of velocity and direction of propagation (perpendicular to wavefront angle) to be ascertained. When averaging occurred in parallel to the wave front, the average intensity was much higher than at any other angle (*C*), resulting in a higher proportion of brighter pixels when plotted as a frequency histogram (*D*). The wave fronts often appeared to be curved, demonstrated by discrete bright areas where the angle of averaging was parallel to the wavefront whilst neightbouring areas were not parallel.

much smaller amplitude in ICC-IM-like cells than in ICC-MY cells (35.3 ± 5.3% of peak fluorescence in ICC-IM compared to 100% peak fluorescence in ICC-MY, $n = 4$; Fig. 6, ICC-IM). After the initial Ca^{2+} wave, intracellular secondary Ca^{2+} waves were often superimposed upon a background increase in Ca^{2+} in ICC-IM-like cells, after a delay of 1–2 s. Unlike *trans* network propagation of the initial Ca^{2+} transients, the intracellular secondary waves propagated slowly through ICC-IM-like cells creating tell-tale diagonal streaks in spatio-temporal maps (Fig. 7).

Pharmacology of Ca^{2+} transients

Addition of tetrodotoxin (TTX: 1 μM; $n = 4$) did not block Ca^{2+} transients in ICC-MY, but in some preparations TTX caused slowing of frequency (i.e. interval increased on average 17.3%; Control 12.47 ± 0.54 s compared to TTX 15.07 ± 0.58 s; $P < 0.05$; $n = 3$; Fig. 8*A*). This suggests that generation of this activity does not depend upon neural input, but spontaneous release of neurotransmitters may affect the frequency. It should be noted that both inhibitory and excitatory neurotransmitters have profound effects on

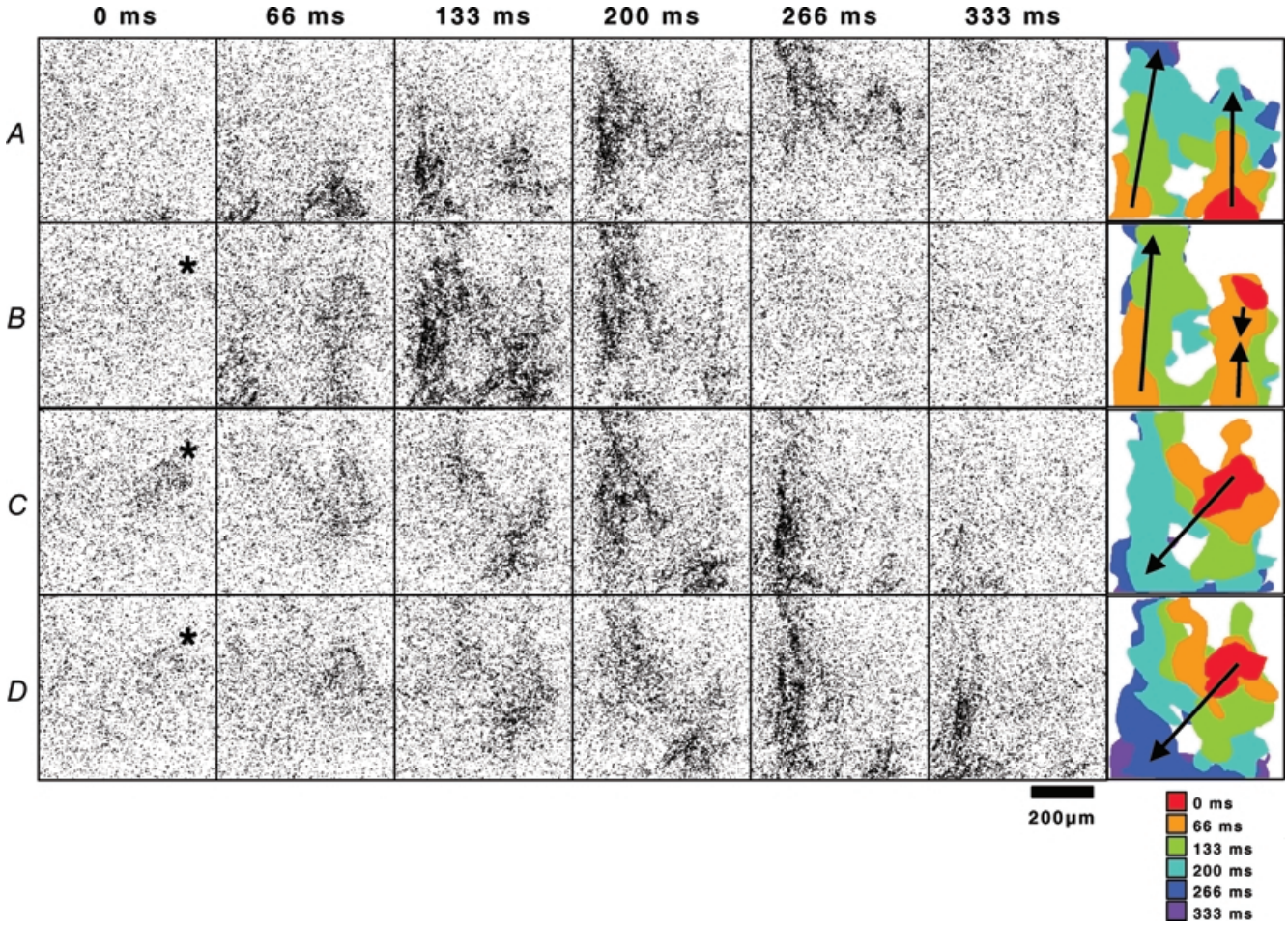

Figure 4. Origin and propagation of Ca^{2+} waves in an ICC-MY network
A–D show the progression of four sequential Ca^{2+} waves. In *A* a wave emerges from the lower edge (0 ms) and propages toward the top of the images within 330 ms. In *B–D* a site of origin occurred within the field of view. Waves emerged in three successive cycles in the upper right quandrant (below and to the left of the asterisk). In *B* the emergent pacemaker event collided with a wave coming from the previous dominant site and was anihilated in the right upper quandrant in subsequent images. The previously utilized pathway along the left side of the field of view was preserved. In *C–D* the pacemaker in the upper right quandrant became regionally dominant and waves propagated radially toward the bottom left corner for 2 cycles. Coloured topological representations were constructed by applying a median filter to each thresholded frame, then regions of high fluorescence were manually outlined and colour-coded to denote the sequence of activation (from time of origin (red) to termination (purple; see colour key)). Active regions from each frame were stacked as a single image and arrows show the overall direction of spread of activity.

the intrinsic frequency of gastric antral ICC-MY (Kim *et al.* 2002, 2003), even though it is ICC-IM, rather than ICC-MY, that appear to be functionally innervated (Dickens *et al.* 2000; Ward *et al.* 2000; Hirst *et al.* 2002*b*). Addition of 2-APB (25 μM; $n = 3$), an agent known to block IP_3 receptor-operated Ca^{2+} release (see Discussion in Hennig *et al.* 2002), blocked Ca^{2+} transients (Fig. 8*A*), suggesting that release of Ca^{2+} from intracellular stores is required for the initiation of Ca^{2+} transients in ICC-MY (Kito & Suzuki, 2003). Nicardipine (2 μM), to block L-type Ca^{2+} channels, consistently and rapidly abolished the slow Ca^{2+} transients in smooth muscle cells, but Ca^{2+} transients in ICC-MY were not blocked (Fig. 8*B*). The resistance to nicardipine of transients in ICC-MY is consistent with the lack of sensitivity of pacemaker activity to L-type Ca^{2+} channel blockers in the guinea-pig stomach (Dickens *et al.* 1999).

Discussion

In the present study we measured Ca^{2+} transients in cellular elements of gastric smooth muscle tissues. Co-localization of Kit in a subpopulation of cells generating rhythmic fluorescence signals demonstrates that Ca^{2+} transients could be recorded from ICC *in situ*. Both ICC-MY and ICC-IM populations were visualized with Fluo-4. ICC-MY were easy to distinguish due to the relatively strong loading of Fluo-4 into these cells, their distinctive, highly branching morphology, and the organization of these cells into networks through which Ca^{2+} waves

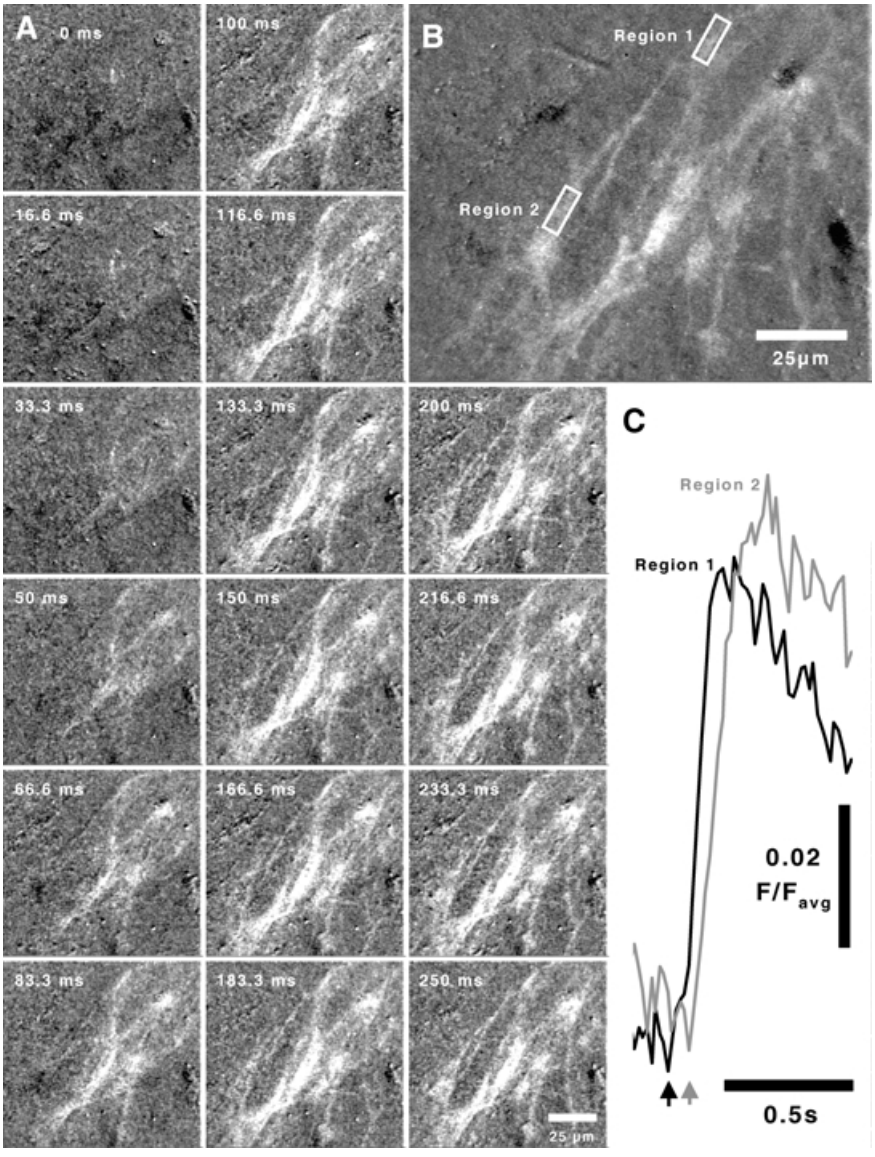

Figure 5. Spatial resolution of ICC-MY during propagation of Ca^{2+} wave
At low magnification it was impossible to discern the morphology of individual ICC-MY (Figs 3 and 4). To be certain that the Ca^{2+} waves observed occurred in cellular elements of the ICC-MY network, waves were also recorded at × 60 magnification. *A* shows the progression of a single Ca^{2+} wave through the ICC-MY network, and the structure of cells is clearly visualized. In the cycle shown in the series of images (0–250 ms), a wave begins at the top right corner and spreads toward the bottom left corner within 50 ms. Fluorescence is sustained in these cells through the rest of the image sequence shown. It should be noted that another region of the network (region 2 in *B*) is activated with some delay from the main group of cells (region 1 in *B*) during this Ca^{2+} wave. *C* shows fluorecence in regions 1 and 2 as a function of time. Arrows at the bottom depict the time at which the 2 regions became active.

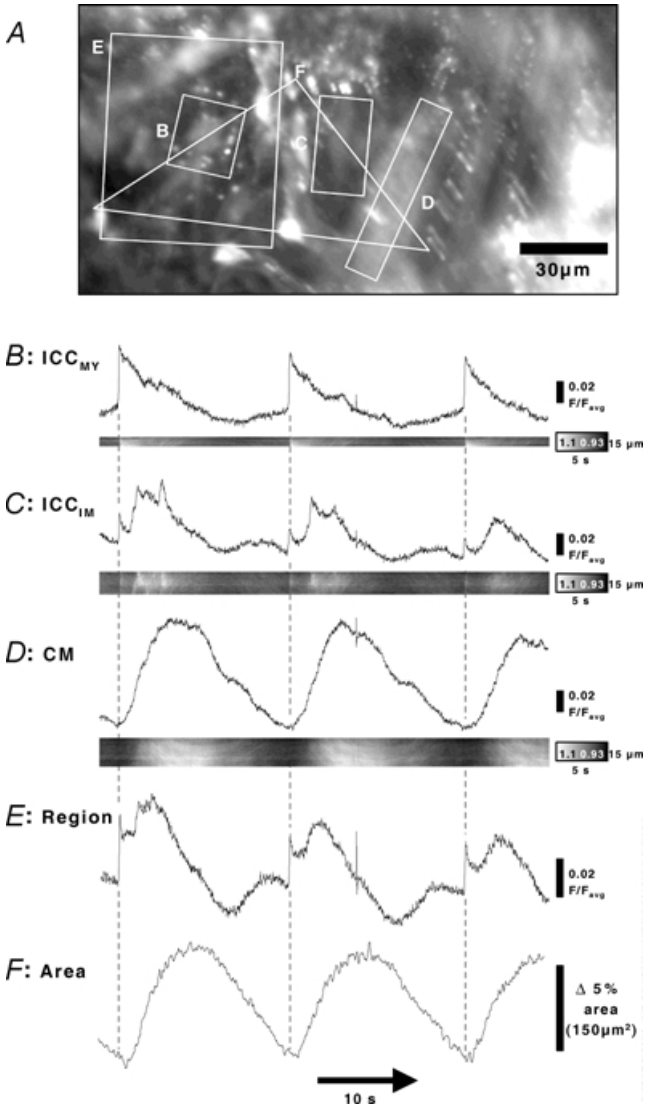

Figure 6. Time course of Ca^{2+} transients in different cells types
Ca^{2+} transients with different wave forms were detected in different cell types. *A* shows a field of view in which a number of cell types were observed. Specific cellular profiles within the areas outlined were used to determine fluorescence changes in different cellular types. *B* shows typical transients obtained from ICC-MY. These events consisted of a rapid upstroke of fluorescence followed by decay back toward the resting level. *C* shows events recorded from cells with the morphology of ICC-IM and these events consisted of an echo of the ICC-MY activity (a rapid upstroke and decay toward resting levels) that were always of smaller in amplitude than the events in ICC-MY. ICC-IM had repetitive Ca^{2+} transients superimposed upon a plateau level. *D* shows the Ca^{2+} wave in an adjacent bundle of circular smooth muscle cells (CM). These cells did not display rapid upstrokes in fluorescence but rather a gradual rise and an extended plateau phase before the resting level was restored. *E* shows Ca^{2+} fluorescence in a field of view with multiple types of cells. The apparent depression in fluorescence during the interval between transients was a movement artifact. *F* shows the change in surface area (or distortion) of the field of view resulting from muscle contraction. Note that the smooth muscle Ca^{2+} wave follows the initiation of activity by ICC-MY, and contraction lags behind the development of the Ca^{2+} transient in the CM.

propagated. ICC-IM also had distinctive morphologies and were aligned with the axis of the circular muscle fibres. These morphologies correspond to the previously described structures of gastric ICC (see Burns *et al.* 1996). The branching morphology of ICC-MY cells provides a means for these cells to propagate events at multiple angles, which facilitates the radial spread of slow waves from the primary site of initiation.

The Ca^{2+} oscillations in ICC-MY occurred without obligatory input from the enteric nervous system at approximately the same frequency as slow waves in the guinea-pig gastric antrum (Hennig *et al.* 1997; Dickens *et al.* 1999), suggesting that these events corresponded to pacemaker activity. Ca^{2+} release from stores in ICC-MY could be a source for initiation of slow waves or amplification of Ca^{2+} transients (Suzuki & Hirst, 1999; Ward *et al.* 2000), but the rate of spread of Ca^{2+} waves through the ICC-MY networks (3.2 mms^{-1}) was at least an order of magnitude too fast for store-dependent Ca^{2+} waves to be responsible for propagation (see Hennig *et al.* 2002). Block of Ca^{2+} waves in ICC-MY by 2-APB is consistent with current models of electrical slow wave generation in which these events are initiated by Ca^{2+} release from IP_3 receptors (Ward *et al.* 2000; Hirst & Edwards, 2001). From the rate of propagation of Ca^{2+} waves through the ICC-MY network, it is likely that an electrical mechanism, possibly involving Ca^{2+} entry, is involved (Lee & Sanders, 1993; Hirst & Edwards, 2001; Kim *et al.* 2002). ICC-MY express both dihydropyridine-sensitive and insensitive voltage-dependent Ca^{2+} conductances (Lee & Sanders, 1993; Kim *et al.* 2002). The fact that Ca^{2+} transients were reduced in magnitude, but not blocked by 2 μM nicardipine, is consistent with the observation that pacemaker activity in the guinea-pig antrum persists in the presence of L-type Ca^{2+} channel blocking drugs (see Hirst & Edwards, 2001) and with the expression of a dihydropyridine-insensitive Ca^{2+} conductance by these cells.

In our experiments we visualized small groups of ICC that were part of a larger ICC-MY network, most of which was out of the field of view. Under these conditions it was rare to visualize the site of initiation of a Ca^{2+} wave, but the direction of spread of Ca^{2+} waves and curvature of the wave front gave an indication of the source of each wave. These observations suggest that the initiation sites of Ca^{2+} waves were unstable and shifted from event-to-event. Spontaneous variation in the site of initiation of Ca^{2+} waves is reminiscent of the cycle-to-cycle changes in the site of pacemaker iniation in the site of slow wave initiation in gastric muscles (Publicover & Sanders, 1984) and ICC-MY (Hirst & Edwards, 2001). Our data suggest there is

no innate specialization in regional networks of ICC-MY that allows one cell to be the dominant pacemaker. These are microscopic observations, however, that should not be confused with the existence of organ-level dominant pacemakers in the stomach and small bowel. Lack of cell-specific dominance at the microscopic level and emergence of region-specific dominance at the organ level suggest that the pacemaker properties of ICC in ICC-MY networks change gradually as a function of anatomical location. ICC in some regions consistently generate slow waves at higher rates. An example of this is the distinct frequency gradient that exists in the stomach from corpus to antrum (Kelly & Code, 1971), and ICC isolated from these regions have distinct frequency characteristics consistent with their roles as dominant and entrainable pacemakers (Ordog *et al.* 2002).

Propagation of pacemaker activity through the ICC-MY network occurred at a velocity consistent with the speed of antral peristaltic waves (Hennig *et al.* 1997), conduction velocity of pacemaker potentials through networks of ICC-MY (Hirst & Edwards, 2001) and that of slow waves recorded from sheets or strips of muscle with multiple electrodes (Publicover & Sanders, 1984). A novel observation of the present study was that propagation was not continuous and linear from cell to cell, but consisted of regions in which events skipped over cells and rates increased and decreased with position. Observations of small groups of cells within the ICC-MY network in which

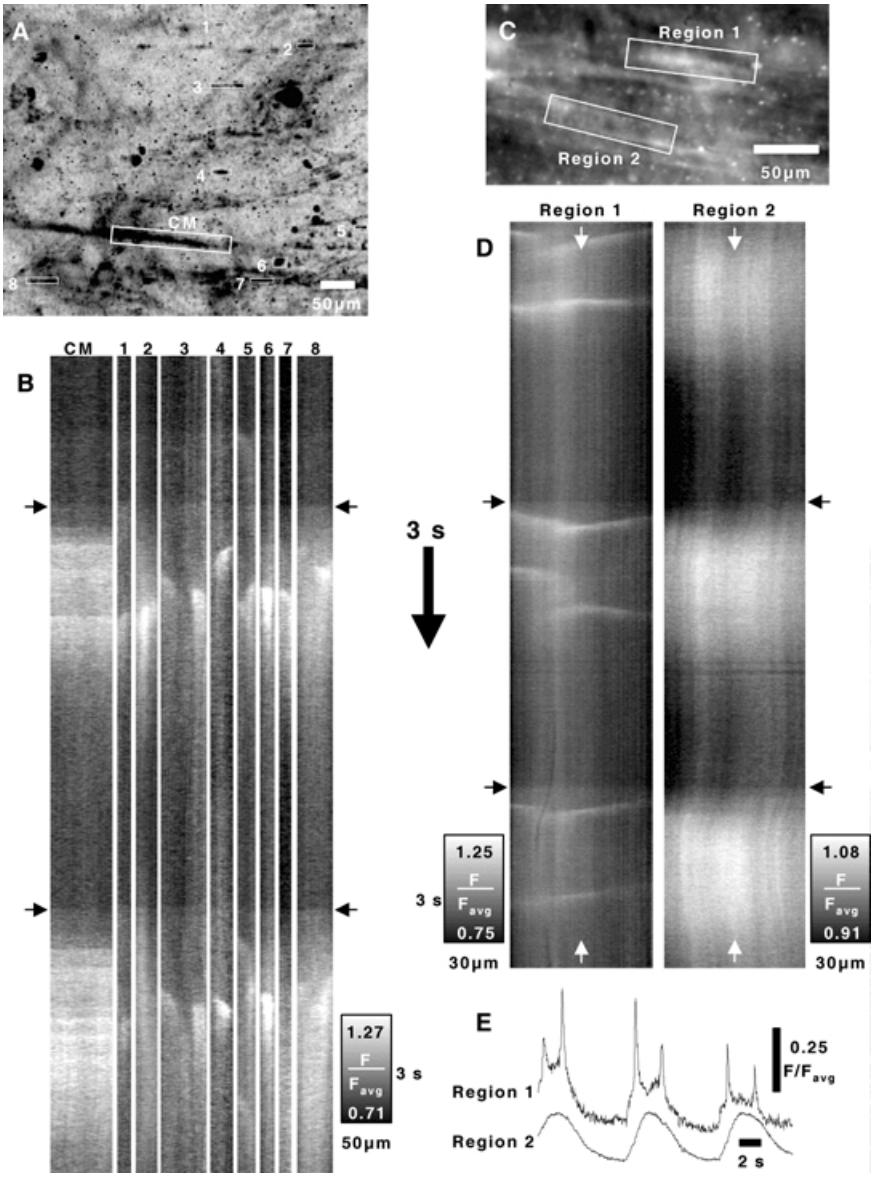

Figure 7. Initiating and secondary Ca^{2+} waves in ICC-IM and CM during the pacemaker cycle
Ca^{2+} waves were often followed by slowly propagating, localized secondary intracellular Ca^{2+} waves in cells with the morphology of ICC-IM. These events were confined to individual cells and propagated at a velocity of approximately 60 μm s^{-1}. *A* shows a field of view in which several ICC-IM-like cells (1–8) and CM cells were visualized. *B*, events in these cells showed up in spatial temporal maps as flashes following an initial Ca^{2+} wave front (indicated by arrows). *C* shows a higher power image of an ICC-IM (region 1) and CM cell (region 2). *D* shows spatio-temporal map of the activty of the cells in *C*. Leading edges of initiating Ca^{2+} waves are indicated by black arrows and secondary intracellular Ca^{2+} waves, occurring after the initial Ca^{2+} wave, appear as bright bands. The secondary Ca^{2+} waves were apparent only during the period of elevated Ca^{2+} following the initiating Ca^{2+} wave. The propagation of secondary intracellular Ca^{2+} varied in frequency and direction (*D*; region 1). *E* shows fluorescence traces of region 1 (ICC-1M) and region 2 (CM) during 3 cycles (between white arrows). Note secondary intracellular Ca^{2+} waves appear as fluorescence peaks in region 1 (ICC-IM).

the sequence of activation was determined showed that the conduction pathway varied from event to event, suggesting that propagation (or entrainment of pacemakers) is, at a microscopic level, stochastic, and may reflect the dynamic excitability of each pacemaker cell within the network. A pacemaker closer to its threshold would tend to be entrained more readily than other, less excitable, cells. Relative excitability or relative refractoriness may vary with time to explain the cycle-to-cycle changes in activation sequence we noted. The excitability and refractory properties of individual ICC-MY or groups of ICC-MY also appeared to generate restrictions or facilitations in the pathway of propagation, and cycle-to-cycle variations generated complex sequences and pathways of propagation in which waves collided or passed each other in various patterns. In spite of heterogenous propagation at the microscopic level, the sequence of propagation at the macroscopic level showed relatively constant directional movement of Ca^{2+} wavefronts that would be consistent with the spread of slow waves and peristaltic waves in sheets of gastric muscles and intact stomachs.

Cells other than ICC-MY were visualized in our experiments. We observed Ca^{2+} transients in smooth muscle cells and in ICC-IM that followed initiation of events in ICC-MY. These data are consistent with the concept that ICC-MY serve as the pacemaker in the guinea-pig antrum (Dickens *et al.* 1999) and that ICC-IM may augment pacemaker depolarizations reaching the circular muscle layer (Dickens *et al.* 2001). Smooth muscle cells were easy to distinguish from the activity of ICC-MY, and the Ca^{2+} transients in muscle cells were typically slowly developing events lasting several seconds. These events were blocked by drugs that block L-type Ca^{2+} channels. In some cases it was difficult to isolate Ca^{2+} transients in ICC-MY and smooth muscle cells because the cells were not spatially separated. Imaging from both cell types simultaneously produced a waveform consisting of a rapid upstroke, followed by a sustained plateau phase as the muscle response increased after the initial upstroke. The activity specific to smooth muscle cells in these images was possible to distinguish because of the slow rising phase of the second (plateau-like) Ca^{2+} transient. Previous studies have demonstrated that Ca^{2+} entry in smooth

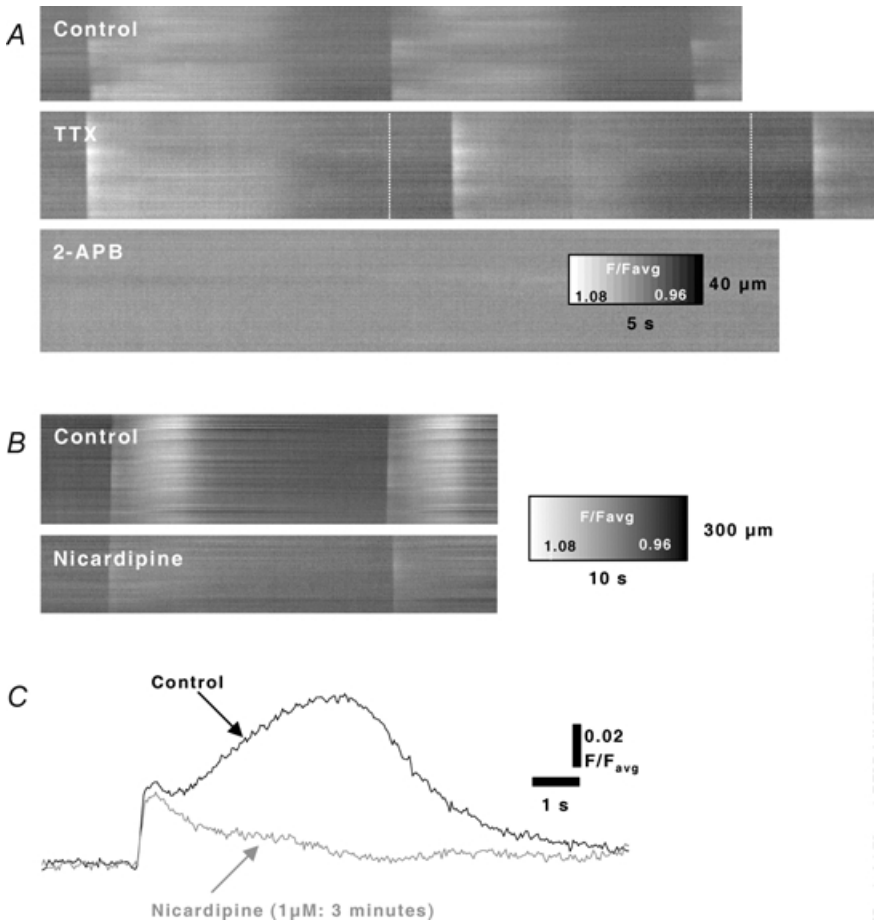

Figure 8. Pharmacology of Ca^{2+} waves
Spatio-temporal maps display Ca^{2+} waves in fields of view (i.e. representing contributions from ICC and CM) before and after TTX (1 μM). TTX did not abolish generation or propagation of Ca^{2+} waves, however, an increase was noted in the period between Ca^{2+} waves (white dashed lines indicate normal period). 2-APB (25 μM) abolished Ca^{2+} waves. *B*, nicardipine (2 μM) reduced the sustained elevation in Ca^{2+} (attributed to CM as in Fig. 6*D*) following the initiating Ca^{2+} wave. *C*, the initial rapid rise in Ca^{2+} fluorescence (attributed to the contribution of ICC-MY as in Figs 1 and 6*B*) was well maintained in the presence of nicardipine.

muscle cells of gastric muscles is primarily due to L-type (dihydropyrdine-resistant) Ca^{2+} channels (Mitra & Morad, 1985; Vogalis *et al.* 1992; Kim *et al.* 1997), which are activated during the slow wave depolarization (see also Ozaki *et al.* 1992). In the present study the increase in Ca^{2+} in muscle cells was followed within 1–2 s by distortion of the tissue, and recoil (cessation of active contraction), which began shortly after peak fluorescence was reached in muscle cells.

Ca^{2+} transients in ICC-IM were characterized by small, fast upstroke transients that occurred in synchrony ($\pm$50 ms) with the major upstroke transient in nearby ICC-MY. The initial upstrokes of Ca^{2+} transients in ICC-IM were always of smaller magnitude than the corresponding events in ICC-MY, but occurred in a highly coordinated manner across a wide field of view. This observation suggests that the initial Ca^{2+} transient in ICC-IM is highly dependent upon the pacemaker activity in ICC-MY. After the upstroke, secondary intracellular Ca^{2+} waves occurred in ICC-IM. Intracellular Ca^{2+} waves have been reported previously in smooth muscle (Gordienko *et al.* 1998; Hennig *et al.* 2002), but always appeared to be continuously and randomly activated in cells within a region of tissue. In the antrum, secondary intracellular Ca^{2+} waves in ICC-IM appear to be dependent upon the pacemaker activity of ICC-MY. The onset of the secondary waves occurred shortly after the upstroke of the initial Ca^{2+} transient, during the period of the sustained Ca^{2+} transients in muscle cells. The role of intracellular Ca^{2+} transients in the ICC-IM during the slow wave cycle is unclear, but it may be related to regulation of ion channels that may amplify or modulate the electrical slow wave activity (Dickens *et al.* 2001).

In conclusion, these results demonstrate that pacemaker activity, as assayed by global Ca^{2+} responses, spreads microscopically in a non-orthogonal fashion through the ICC-MY network in the guinea-pig antrum and involves the stochastic recruitment of adjacent cells to form a macroscopic wavefront. The intracellular Ca^{2+} waves we observed occurred first in ICC-MY and then activated coordinated transients in ICC-IM and smooth muscle cells of both muscle layers. The Ca^{2+} transients in smooth muscle cells were coincident with distortions of the tissue. Pacemaker activity was abolished by a blocker of IP_3 receptor-operated Ca^{2+} stores, but remained after neural blockade and blockade of L-type Ca^{2+} channels. These data demonstrate that cell-specific resolution of Ca^{2+} transients in intact tissues is a powerful technique for studying propagation of activity and determining the sequence of activation in multicellular GI muscles.

References

Bauer AJ, Publicover NG & Sanders KM (1985). Origin and spread of slow waves in canine gastric antral circular muscle. *Am J Physiol* **249**, G800–G806.

Burns AJ, Herbert TM, Ward SM & Sanders KM (1997). Interstitial cells of Cajal in the guinea-pig gastrointestinal tract as revealed by c-Kit immunohistochemistry. *Cell Tissue Res* **290**, 11–20.

Burns AJ, Lomax AE, Torihashi S, Sanders KM & Wards SM (1996). Interstitial cells of Cajal mediate inhibitory neurotransmission in the stomach. *Proc Nat Acad Sci U S A* **93**, 12008–12013.

Cousins HM, Edwards FR, Hickey H, Hill CE & Hirst GDS (2003). Electrical coupling between myenteric interstitial cells of Cajal and adjacent muscle layers in the guinea pig gastric antrum. *J Physiol* **550**, 829–844.

Dickens EJ, Edwards FR & Hirst GDS (2000). Vagal inhibitory projections to rhythmically active cells in the antral region of guinea-pig stomach. *Am J Physiol* **279**, G388–G399.

Dickens EJ, Edwards FR & Hirst GDS (2001). Selective knockout of intramuscular interstitial cells reveals their role in the generation of slow waves in mouse stomach. *J Physiol* **531**, 827–833.

Dickens EJ, Hirst GDS & Tomita T (1999). Identification of rhythmically active cells in guinea-pig stomach. *J Physiol* **514**, 515–531.

Gordienko DV, Bolton TB & Cannell MB (1998). Variability in spontaneous subcellular calcium release in guinea-pig ileum smooth muscle cells. *J Physiol* **507**, 707–720.

Hennig GW, Brookes SJH & Costa M (1997). Excitatory and inhibitory motor reflexes in the isolated guinea-pig stomach. *J Physiol* **501**, 197–212.

Hennig GW, Costa M, Chen BN & Brookes SJH (1999). Quantitative analysis of peristalsis in the guinea-pig small intestine using spatio-temporal maps. *J Physiol* **517**, 575–590.

Hennig GW, Smith CB, O'Shea DM & Smith TK (2002). Patterns of intracellular and intercellular Ca^{2+} waves in the longitudinal muscle layer of the murine large intestine in vitro. *J Physiol* **543**, 233–253.

Hirst GDS, Beckett EAH, Sanders KM & Ward SM (2002*a*). Regional variation in contribution of myenteric and intramuscular interstitial cells of Cajal to generation of slow waves in mouse gastric antrum. *J Physiol* **540**, 1003–1012.

Hirst GDS, Dickens EJ & Edwards FR (2002*b*). Pacemaker shift in the gastric antrum of guinea-pigs produced by excitatory vagal stimulation involves intramuscular interstitial cells. *J Physiol* **541**, 917–928.

Hirst GDS & Edwards FR (2001). Generation of slow waves in the antral region of guinea-pig stomach – a stochastic process. *J Physiol* **535**, 165–180.

Horiguchi K, Semple GSA, Sanders KM & Ward SM (2001). Distribution of pacemaker function through the tunica muscularis of the canine gastric antrum. *J Physiol* **537**, 237–250.

Huizinga JD, Thuneberg L, Kluppel M, Malysz J, Mikkelsen HB & Bernstein A (1995). W/kit gene required for intestinal cells of Cajal and for intestinal pacemaker activity. *Nature* **373**, 347–349.

Kelly KA & Code CF (1971). Canine gastric pacemaker. *Am J Physiol* **220**, 112–118.

Kim SJ, Ahn SC, Kim JK, Kim YC, So I & Kim KW (1997). Changes in intracellular Ca^{2+} concentration induced by L-type Ca^{2+} channel current in guinea pig gastric myocytes. *Am J Physiol* **273**, C1947–C1956.

Kim TW, Beckett EA, Hanna R, Koh SD, Ordog T, Ward SM & Sanders KM (2002). *Regulation* of pacemaker frequency in the murine gastric antrum. *J Physiol* **538**, 145–157.

Kim TW, Koh SD, Ordog T, Ward SM & Sanders KM (2003). Muscarinic regulation of pacemaker frequency in murine gastric interstitial cells of Cajal. *J Physiol* **546**, 415–425.

Kito Y, Fukuta H & Suzuki H (2002). Components of pacemaker potentials recorded from the guinea pig stomach antrum. *Pflugers Arch* **445**, 202–217.

Kito Y & Suzuki H (2003). Electrophysiological properties of gastric pacemaker potentials. *J Smooth Muscle Res* **39** (5), 163–173.

Langton P, Ward SM, Carl A, Norell MA & Sanders KM (1989). Spontaneous electrical activity of interstitial cells of Cajal isolated from canine proximal colon. *Proc Nat Acad Sci U S A* **86**, 7280–7284.

Lee HK & Sanders KM (1993). Comparison of ionic currents from interstitial cells and smooth muscle cells from the canine colon. *J Physiol* **460**, 135–152.

Mitra R & Morad M (1985). Ca^{2+} and Ca^{2+} -activated K^+ currents in mammalian gastric smooth muscle cells. *Science* **229**, 269–272.

Nose K, Suzuki H & Kannan H (2000). Voltage dependency of the frequency of slow waves in antrum smooth muscle of the guinea-pig stomach. *Jap J Physiol* **50**, 625–633.

Ordog T, Baldo M, Danko R & Sanders KM (2002). Plasticity of electrical pacemaking by interstitial cells of Cajal and gastric dysrhythmias in W/W mutant mice. *Gastroenterology* **123**, 2028–2040.

Ordog T, Ward SM & Sanders KM (1999). Interstitial cells of cajal generate electrical slow waves in the murine stomach. *J Physiol* **518**, 257–269.

Ozaki H, Blondfield DP, Hori M, Sanders KM & Publicover NG (1992). Cyclic AMP-mediated regulation of excitation-contraction coupling in canine gastric smooth muscle. *J Physiol* **447**, 351–372.

Publicover NG & Sanders KM (1984). A technique to locate the pacemaker in smooth muscles. *J Appl Physiol* **57**, 1586–1590.

Sanders KM (1996). A case for interstitial cells of Cajal as pacemakers and mediators of neurotransmission in the gastrointestinal tract. *Gastroenterology* **111**, 492–515.

Sanders KM & Publicover NG (1989). Electrophysiology of gastric muslces. In *Handbook of Physiology: the Gastrointestinal System*, **vol. 1**, ed.Schultz SG, pp. 187–216. Oxford University Press, New York.

Stevens FJ, Publicover NG & Smith TK (1999). Induction and organization of Ca^{2+} waves by enteric neural reflexes. *Nature* **399**, 62–66.

Stevens RJ, Publicover NG & Smith TK (2000). Propagation and neural regulation of calcium waves in longitudinal and circular muscle layers of guinea pig small intestine. *Gastroenterology* **118**, 892–904.

Suzuki H & Hirst GDS (1999). Regenerative potentials evoked in circular smooth muscle of the antral region of guinea-pig stomach. *J Physiol* **517**, 563–573.

Tomita T (1981). Electrical activity (spikes and slow waves) in gastrointestinal smooth muscles. In *Smooth Muscle: an Assessment of Current Knowledge*, ed.Bulbring E, Brading AF, Jones AW & Tomita T, pp. 127–156. Edward Arnold, London.

Torihashi S, Ward SM, Nishikawa S, Nishi K, Kobayashi S & Sanders KM (1995). C-kit-dependent development of interstitial cells and electrical activity in the murine gastrointestinal trace. *Cell Tissue Res* **280**, 97–111.

Vogalis F, Publicover NG & Sanders KM (1992). *Regulation* of calcium current by voltage and cytoplasmic calcium in canine gastric smooth muscle. *Am J Physiol* **262**, C691–C700.

Ward SM, Burns AJ, Torihashi S & Sanders KM (1994). Mutation of the proto-oncogene c-kit blocks development of interstitial cells and electrical rhythmicity in murine intestine. *J Physiol* **480**, 91–97.

Ward SM, Ordog T, Koh SD, Bakers SA, Jun JY, Amberg G, Monaghan K & Sanders KM (2000). Pacemaking in interstitial cells of Cajal depends upon calcium handling by endoplasmic reticulum and mitochondria. *J Physiol* **525**, 355–361.

Yamazawa T & Iino M (2002). Simultaneous imaging of Ca^{2+} signals in interstitial cells of Cajal and longitudinal smooth muscle cells during rhythmic activity in mouse ileum. *J Physiol* **538**, 823–835.

Acknowledgements

This project was supported by P01 DK 41315 to K.M.S. and T.K.S., and by DK 40569 to K.M.S. and S.M.W. G.W.H. is a CJ Martin Postdoctoral Research Fellow (NH & MRC, Australia). G.D.S.H. is supported by NH & MRC, Australia. Part of the imaging and analysis was performed by an Imaging Core Laboratory supported by a COBRE grant P20 RR 018751–01.

Author's present address

G. D. S. Hirst: Division of Neuroscience, John Curtain School of Medicine Research, A.N.U., Acton, 2601, Australia.

Image processing appendix

Contrast and brightness adjustments were applied to each image or spatio-temporal map. In spatio-temporal maps, the relative fluorescence ratios were displayed in the calibration box.

Abbreviations

MS = motion stabilized
T_{avg} (s) = time averaged (time in seconds)
BS = background subtracted (average image of entire image sequence used)
DI = de-interlaced
DT (s) = differentiated (timestep between images in seconds)
MF = median filtered (3 × 3 ' + ' median filter)
s.d. = standard deviation of change in pixel intensity in entire image sequence
T = thresholded
I = inverted
PC = pseudo-coloured (red/green)

Figure 1

A, B, D: MS, T_{avg}(4 s), PC(red).
C: MS, BS, T_{avg}(1 s), MF, PC(green).
E: MS, BS, T_{avg}(0.2 s), MF.

Figure 2

C: MS, DT(0.18 s), T_{avg}(0.09 s), MF.

Figure 3

A, B: MS, DT(0.16 s), T, I.

Figure 4

A-D: DI, MS, DT(0.16 s), T, I.
Coloured: (as per *A–D*) + MF, manual outlining.

Figure 5

A: DI, MS, BS, MF.
B: MS, BS, T_{avg}(0.3 s).

Figure 6

A: MS, T_{avg}(3 s).

Figure 7

A: s.d.
C: MS, T_{avg}(3 s)